1-1-2019

Stability analysis and design charts for a sandy soil slope supporting an embedded strip footing

Emmanuel Baah-Frempong
Edith Cowan University, e.baahfrempong@ecu.edu.au

Sanjay Kumar Shukla
Edith Cowan University, s.shukla@ecu.edu.au

10.1186/s40703-018-0082-2
Baah-Frempong, E., & Shukla, S. K. (2018). Stability analysis and design charts for a sandy soil slope supporting an embedded strip footing. International Journal of Geo-Engineering, 9(1), 13. Available here.

Baah-Frempong and Shukla *Geo-Engineering (2018)9:13*
https://doi.org/10.1186/s40703-018-0082-2

International Journal of Geo-Engineering

ORIGINAL RESEARCH Open Access

Stability analysis and design charts for a sandy soil slope supporting an embedded strip footing

Emmanuel Baah-Frempong* and Sanjay Kumar Shukla

*Correspondence:
e.baahfrempong@ecu.edu.au
School of Engineering, Edith Cowan University, Joondalup, Perth, Australia

Abstract

In several field situations, especially in the hilly terrains, the construction of footings on slopes becomes essential. The factor of safety of a slope supporting a loaded footing on the crest is dependent on the position of the footing from the crest edge. Most studies in the past have focused on analysing the bearing capacity and settlement behaviour of a footing resting on a slope crest, but foundations in most infrastructure projects are usually built at some depth below the ground surface. Therefore, the availability of some form of design charts for determining the factor of safety of a slope supporting an embedded footing will be highly useful for the practising engineers. In the current work, the finite element analysis of a sandy soil slope supporting an embedded footing was carried out using the Plaxis 2D, a finite element-based commercial software, in order to examine the effect of slope geometry, soil properties, and footing locations on the stability of slope in terms of factor of safety. The results of the analysis show that the factor of safety of the slope increases with an increase in the footing edge distance, footing depth and soil relative density, but it decreases with an increase in the slope angle and applied pressure on the footing. Some design charts have been developed along with an illustrative example to explain how these charts can be used by the practising engineers.

Keywords: Factor of safety, Slope stability, Strength reduction technique, Failure zone

Introduction

The stability analysis of slopes has been a challenging task for geotechnical engineers since ancient days. In assessing the stability of any slope, the focus is mainly on calculating the factor of safety to estimate the degree of closeness of the slope from the failure condition. Some infrastructure projects, particularly in hilly terrains, involve the construction of footings/foundations on slopes. When a foundation is built on a slope, the factor of safety is expected to reduce depending on the foundation location relative to the crest edge and its depth. In the past, several studies have been carried out on the bearing capacity and settlement behaviour of footings resting on unreinforced slopes. Some investigators have developed analytical formulations to estimate the bearing capacity of a footing positioned on a slope [1–6]. Meyerhof [4] developed an analytical formulation to estimate the bearing capacity of a footing on a slope face and crest for both completely cohesive and cohesionless soils. For a footing on top of the slope, it

was reported that the bearing capacity factors decreased with higher slope inclination and increased with the footing distance from the slope edge. The bearing capacity of the footing is independent of the slope angle when the footing is located at a distance, greater than 2–6 times the footing width, from the slope crest edge. Graham et al. [3] used the stress characteristics to analyse the load-bearing pressure of a footing on cohesionless soil slope. They compared their results with the experimental data of Shields et al. [7] and found a good agreement between them. Saran et al. [6] used the limit equilibrium and limit analysis methods to obtain the bearing capacity of a foundation close to a slope. It was demonstrated that the two methods produced almost the same results presented in the form of non-dimensional bearing capacity factors which are influenced by the soil friction angle, slope inclination and footing edge distance. Narita and Yamaguchi [5] carried out a log-spiral analysis of the bearing capacity of footings located on slopes. They compared their results with other analytical and experimental works and found that the method overestimates the bearing capacity in comparison to other analytical solutions. A good agreement was however observed between the ultimate bearing capacity and the form of failure surface from the log spiral analysis and the laboratory model test. Buhan and Garnier [1] analysed the load bearing behaviour of a footing close to a slope by the yield design theory and compared the predictions with a full scale and a centrifuge test results. Castelli and Motta [2] utilised the limit equilibrium method to investigate the load bearing capacity of a foundation on a ground surface with a slope. A parametric study, under static and seismic conditions, was conducted to examine the effect of footing edge distance, slope inclination, footing embedment depth and seismic coefficients on the footing load bearing pressure.

Some investigators have analysed the bearing capacity of footings on slopes by laboratory model tests [8–10]. Castelli and Lentini [8] experimentally evaluated the load-bearing behaviour of footings on slopes, and proposed modified bearing capacity factors by considering the effect of sloping ground. Keskin and Laman [9] studied the bearing capacity of a strip footing positioned on a sand slope. They demonstrated that the ultimate bearing capacity improved with an increase in the footing edge distance, sand relative density, and decrease in slope inclination. Patil and Chore [10] demonstrated that the bearing capacity of a strip footing on a fly ash and furnace slag slope is influenced by the footing edge distance and slope angle. They also established a good agreement between the ultimate bearing capacity obtained from the experimental work and analytical solution.

Numerical modelling has also been utilised by some researchers to study the bearing capacity of footings on slopes [9, 11–13]. Georgiadis [12] presented a finite element analysis of the load-carrying capacity of foundations situated on slopes and compared the results with available analytical methods. Keskin and Laman [9] validated the results from their laboratory test with a numerical modelling data. Archaryya and Dey [11] numerically studied the collapse process and bearing capacity of a foundation on top of a slope that has no cohesion. They analysed the relationship between the footing bearing capacity and the following parameters: internal friction angle of the soil, slope angle, footing embedment depth, footing width, unit weight of the soil and elastic modulus of the soil. Zhou et al. [13] analysed the load-bearing capacity and collapse process of an axially loaded footing on slopes and established six types of collapse.

Most of the past studies have analysed the case of a footing on top of a slope. However, in most infrastructure projects, footings are usually built at some depth below the ground surface; and in the case of sloping ground below the slope crest. Therefore, the analysis of the behaviour of footings embedded in slopes will give the geotechnical/civil engineers more insight into the design of such foundations. There are however very few experimental studies on embedded strip footings supported by slopes [7, 14]. Shields et al. [7] performed a laboratory test to analyse the load bearing pressure of a footing placed on and below the crest of a sand slope constructed in a large tank having a length, width and height of 15 m, 2 m and 2.2 m, respectively. Bauer et al. [14] conducted a laboratory experiment to extend the work of Shields et al. [7]. They investigated the effect of the footing width and inclined applied load on the bearing capacity of the footing at different locations below the crest and face of a dense sandy slope. The test was conducted in a tank having the same internal dimensions as that used by Shields et al. [7].

Previous investigations on the performance of a footing on or in a slope have mainly focused on the bearing capacity and settlement characteristics of the footing, but the behaviour of a footing on or in a slope is governed either by the bearing capacity of the footing or the overall stability of the slope. A combination of the footing bearing capacity behaviour and the slope stability analysis will enable the engineers to gain a better understanding of the design of a footing-slope system. It is widely known that a number of studies have been conducted on the stability of unreinforced slopes/embankments with and without a footing/surcharge load on the crest. However, the literature reveals that the stability analysis of slopes, in terms of factor of safety, carrying embedded footing loads have not been greatly investigated. Also, the stability charts for such slopes are not available. Therefore, in this paper, an attempt is made to develop a numerical model to analyse the stability of a sandy soil slope supporting an embedded footing subjected to loads. The objective of this work is to establish the relationship between the factor of safety of the slope and the following slope and footing parameters: soil properties, slope inclination, footing locations, and applied pressure to the footing. The pattern of failure surfaces developed with respect to the footing locations and applied pressure have also been analysed. Additionally, some practical design charts have been developed for the routine use by the practising engineers.

Slope geometry and foundation details

The geometry of the slope and foundation details used in the present study are illustrated in Fig. 1. The slope has a height H and angle of inclination to the horizontal β. A vertical load is applied to the footing having a width B and located at a distance e from the crest edge with an embedment depth D below the crest. The load applied to the footing is translated to a pressure q at the base of the footing. The slope comprises of a sandy soil with a limited cohesion. It has a unit weight γ, cohesion c and angle of internal friction ϕ. The slope is compacted to various density states expressed in terms of relative density D_r. A preliminary analysis indicated that a berm width (2–14 m) and a foundation thickness (2–14 m) has a negligible effect on the numerical modelling. Consequently, a berm width of 10 m and foundation layer thickness of 10 m was adopted for this study to ensure that the failure surfaces developed remain within the slope boundary. It should be noted that other researchers while analysing the stability of unreinforced and reinforced

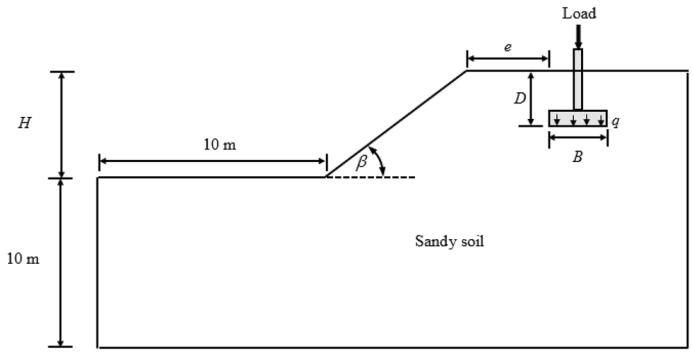

Fig. 1 Geometry of the slope used in the study

slopes, by numerical modelling, utilized berm width and foundation thickness ranging from 5 to 15 m [15–18].

Numerical simulation

A series of two-dimensional finite element slope stability analysis was conducted on a slope supporting an embedded footing (Fig. 1), using Plaxis 2D (2016) software. Plaxis 2D has been developed for the analysis of various geotechnical engineering problems, including slope stability assessment [19]. The finite element analysis has been utilised by many researchers, including Chok et al. [20], for slope stability evaluation. The factor of safety modelling, in Plaxis 2D, utilizes five sequential modes, namely soil, structures, mesh, flow condition and staged construction. The software has several models to simulate soil behavior. Out of these, the Mohr–Coulomb model (MC model), which is an elasto-plastic model and first-order of approximation of soil behavior, was selected due to the availability of required data [21, 22]. The MC model requires six input parameters, namely Young modulus of elasticity (E), Poisson's ratio (μ), total unit weight (γ), friction angle (ϕ), cohesion (c), and dilatancy angle (ψ). Griffiths and Lane [23] observed that, using $\psi = 0$ allowed a model to predict a reliable factor of safety, and a realistic form and position of the potential failure surface. They further noted that E and μ had a negligible influence on the predicted factor of safety. This observation was substantiated by Hammah et al. [24] when they investigated the effect of E (2000–200,000 kPa), μ (0.2–0.48) and ψ (0–35) on the factor of safety of a homogeneous soil slope. Cheng et al. [25] have also found that ψ and E are not sensitive to the factor of safety calculation and concluded that these parameters are not important in the slope stability analysis. Therefore, $\psi = 0$, $\mu = 0.3$ and $E = 30,000$ kN/m^2 have been adopted for the present study. According to Griffiths and Lane [23], the most critical parameters required for the stability assessment of a slope by finite element method are the soil unit weight, friction angle and cohesion. The footing was modelled as an elastic beam element using the "create plate" option in the structures mode of the software. The "create plate" option is utilised to specify the footing properties, including the flexural rigidity EI and normal stiffness EA.

Plaxis 2D has five options for mesh generation ranging from very coarse to very fine, with the medium mesh being the default. Preliminary analysis was conducted to determine and reduce the effect of mesh on the finite element modelling. The boundary conditions set for the model restrained the vertical boundary horizontally and the

bottom horizontal boundary in both vertical and horizontal directions. The slope surface is not horizontal, therefore the primary state of stress was determined by using a gravity force due to the soil mass. The finite element stability analysis uses the strength reduction technique, also known as the strength reduction method, to calculate the factor of safety [23]. In this method, the original strength parameters, c and ϕ, of the soil are reduced by dividing them by a factor called the strength reduction factor (SRF). As the SRF increases, the slope soil strength gradually reduces until the slope attains the state of equilibrium. The value of SRF at the equilibrium state is considered as the factor of safety of the slope. The factored or reduced shear strength parameters c_f and ϕ_f are expressed as follows:

$$c_f = \frac{c}{SRF} \tag{1}$$

$$\phi_f = \tan^{-1}\left(\frac{\tan\phi}{SRF}\right) \tag{2}$$

It should be noted that the SRF is represented as the incremental multiplier $\left(\sum Msf\right)$ in Plaxis 2D. When the value of $\left(\sum Msf\right)$ obtained during the analysis is generally constant for a number of successive steps, then a limit equilibrium state has fully been attained.

Validation of the numerical model

The present study, as already mentioned, is focused on assessing the factor of safety of an unreinforced slope supporting an embedded footing. The literature has revealed that numerous experimental data on the deformation of unreinforced slopes have been reported, but the literature on the stability analysis of such slopes, in terms of factor of safety, is not available. There is, however, a very limited laboratory (centrifuge) test data reported on the deformation and factor of safety of a geosynthetic-reinforced sand slope. It should be noted that most factor of safety analysis of slopes are based on either the limit equilibrium or numerical methods. As a result, some investigators have validated their works with published numerical data [26–28]. Therefore, the validity of the numerical simulations utilized in this study has been verified by using the finite element method to predict the load-settlement behaviour of a footing resting on an unreinforced slope as reported by Gill et al. [29] as well as the failure surface and associated factor of safety of a geotextile-reinforced slope from a centrifuge test data reported by Zornberg et al. [30, 31].

Validation with failure surface and factor of safety data

Zornberg et al. [30, 31] conducted a centrifuge test on a geotextile-reinforced sand slope and determined the factor of safety of the slope at various acceleration levels. This reinforced slope has been employed for the numerical model validation because there is no experimental reported data, to the best knowledge of the authors, on the factor of safety of unreinforced slopes. The slope used by Zornberg et al. [30, 31] has a height $H = 228$ mm and inclination angle $\beta = 63°$. Underlying the slope is a sand foundation layer with a thickness $H = 25.4$ mm. Eighteen geotextiles having an equal length $L = 203$ mm were installed at an equal vertical interval of 12.7 mm below the slope crest.

The sand used for the slope and foundation construction was compacted to a relative density $D_r = 55\%$ with a corresponding friction angle $\varphi = 35°$. A wide-width tensile test, carried out, on the geotextile resulted in an ultimate tensile strength of 0.063 kN/m at 17.7% strain. A 2-dimensional finite element model was developed, using Plaxis 2D package, as well as the sand and geotextile properties reported by Zornberg et al. [30, 31] to predict the failure surface and factor of safety of the slope at failure. The size of the slope, as reported by Zornberg et al. [30, 31], was increased by a scale factor of 10 for the purpose of modelling. Figure 2 compares the slip surfaces obtained from the present study and that of Zornberg et al. [30, 31]. It can be noticed that the results are in good agreement. Also, the factor of safety of 0.99 calculated from the current study is comparable to the factor of safety of 0.9 determined by Zornberg et al. [30], for the slope at failure.

Validation with load-settlement data

Gill et al. [29] investigated the performance of a footing on an unreinforced fly ash slope. The test was performed in a masonry tank having internal dimensions of 2400 mm (length), 310 mm (width) and 1200 mm (depth). The fly ash used for the study comprise 4% clay, 68% silt and 28% sand. It was compacted to a maximum dry unit weight (MDU) of 9.34 kN/m^3 at an optimum moisture content (OMC) of 48%. An unconsolidated undrained triaxial test conducted on the fly ash at MDU state resulted in a cohesion, $c = 20$ kPa and an angle of internal friction, $\varphi = 14°$. The slope was constructed to a height, $H = 750$ mm from the base of the tank and an angle, $\beta = 45°$ to the base of the tank. A 2-dimensional finite element numerical model was established in this study to represent the load-settlement behaviour of the footing, having a width, $B = 100$ mm and located at an edge distance, D_e to width ratio, $D_e/B = 1$, on the fly ash slope crest as reported by Gill et al. [29]. The fly ash was modelled using the MC model with the strength parameters reported by Gill et al. [29]. It should be noted that the MC model, as stated in the previous section, is the first-order of approximation of the behaviour of soil. It assumes the soil stiffness to be constant and for that reason does not take into account the stress nor strain dependency of the soil stiffness during the soil deformation. Figure 3 compares the load-settlement data of the footing from the laboratory experiment [29] and the numerical modelling (present study). It can be observed that the numerical

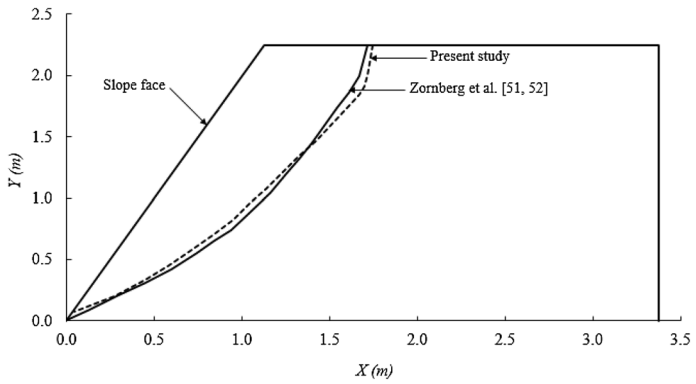

Fig. 2 Comparison of failure surfaces between the present study and works of Zonberg et al. [30, 31]

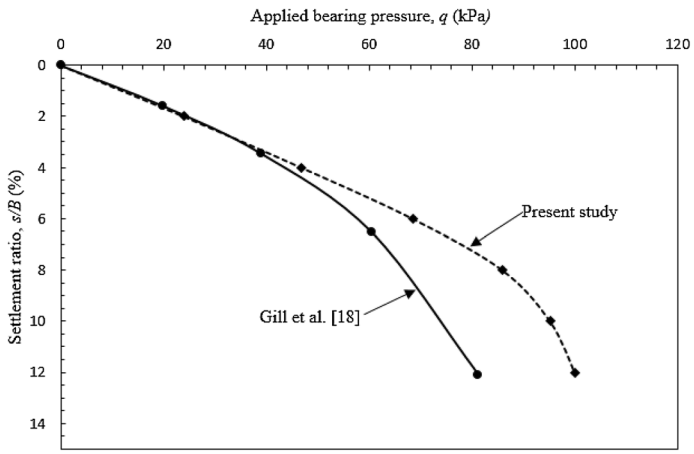

Fig. 3 Comparison of load-settlement curves from Gill et al. [29] and the present study

Table 1 Parameters used in the numerical analysis

Parameter	Values		
Slope			
Angle (°)	40, 50, 60		
Height (m)	6		
Relative density (%)	50	70	90
Total unit weight (kN/m^3)	14.88	15.30	15.78
Cohesion (kPa)	3.75	6.5	7.25
Internal friction angle (°)	36	37	38
Footing			
Width (m)	1.0		
Normal stiffness (kN/m)	5,000,000		
Flexural rigidity (kN/m^2/m)	8500		

results closely agree with the experimental results for low settlements, particularly for $s/B < 4\%$ within the limitations of the MC model used for the modelling. Kazi et al. [32, 33] validated their experimental works on the load-settlement analysis of a footing on unreinforced and geotextile-reinforced sand bed using Plaxis 2D along with the MC model, and also found that the numerical and experimental results match for lower settlements.

Results and discussion

After validating the numerical simulation, a parametric study was conducted to analyse the effect of the following factors on the stability, defined in terms of factor of safety (F), of the sandy slope supporting the embedded footing loads, as presented in Fig. 1: slope angle (β), sand relative density (D_r), footing edge distance (e), footing depth (D) and applied footing pressure (q). The properties of the slope and footing used for the numerical modelling are presented in Table 1. The unit weight and strength parameters of the slope were adopted from laboratory test data reported by Kazi et al. [32, 33]. The correlation of the slope soil relative density D_r with the cohesion c and friction angle ϕ,

based on the laboratory test results in Table 1, are presented in Fig. 4a, b, respectively. The line in Fig. 4a can be described by the following equation:

$$D_r = 10.307c + 9.8773 \quad (R^2 = 0.9018) \tag{3}$$

The line in Fig. 4b may be presented in the equation:

$$D_r = 20\phi - 670 \quad (R^2 = 1) \tag{4}$$

As the values of R^2 for the correlations in Eqs. (3) and (4) are close to unity and equal to 1, respectively, the equations can be used to reasonably estimate the relative density of sands with similar properties as those used in the present study.

Although numerous data have been generated from several analyses, in this study, typical results have been presented and discussed in the subsequent sections. It should be pointed out that a slope height $H = 6$ m and a footing width $B = 1$ m were kept constant in all the analysis in the present work.

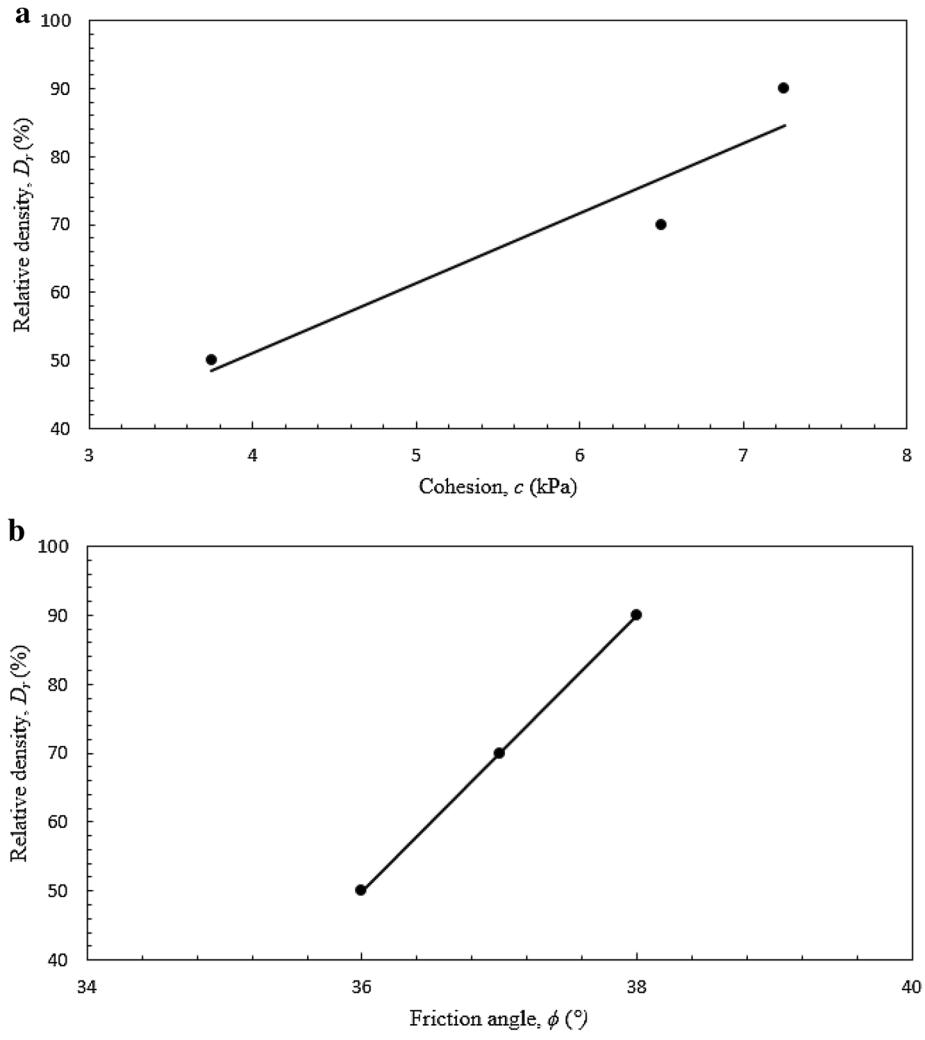

Fig. 4 Correlation of the slope soil relative density, D_r with: **a** cohesion, c, **b** friction angle, φ

Effect of footing depth and applied pressure

The effect of the footing embedment depth D on F was investigated for the slope with $\beta = 40°$, $50°$, $60°$, $H = 6$ m and $D_r = 70\%$. In this analysis, the depth of the footing, with a width $B = 1$ m, was varied at depth ratios $D/B = 0.0$, 0.5, 1.0, 1.5, 2.0, 2.5 for each edge distance ratio $e/B = 0$, 1, 2, 3, 4. It should be noted that $D/B = 0$ and $e/B = 0$ represent the footing on the slope crest and crest edge, respectively. The values of q varying between 0 and 240 kPa were applied to the footing for each combination of depth and edge distance ratio to observe the stability of the slope. A typical finite element model with mesh and boundary conditions is presented in Fig. 5. The variation of F with D/B for the footing at $e/B = 0$ and $e/B = 2$ for the 40° and 50° slopes are, respectively, shown in Figs. 6 and 7. It is observed that F increases with increasing D/B for all the slope angles and footing edge distance. A similar trend on the bearing capacity of a sand slope carrying an embedded footing in a large tank was reported by Shields et al. [7] and Bauer et al. [14]. Although Patra et al. [34] and Shin et al. [35] studied the performance of a footing placed in a sand bed, they as well found that the bearing capacity of the footing increased with increasing D/B.

It is noticed in Figs. 6 and 7 that the rate of improvement in F, generally reduces slightly when the footing is located at $D/B \geq 1$ and $e/B = 0$ as well as at $D/B \geq 0.5$ and $e/B = 2$. It is again observed in Figs. 6 and 7 that the slope behaves as if it is not carrying any footing load ($q = 0$ kPa) when the footing is placed at a certain $e/B > 0$, $D/B > 0$ and $q > 0$. For example, it is demonstrated in Figs. 6a and 7a that locating the footing at $e/B = 0$ and $D/B = 2.5$ and subjecting it to a load $q = 40$ kPa yields almost the same factor of safety as the slope without a footing load. A similar observation is made in Figs. 6b and 7b when the footing is positioned at $e/B = 2$ and $D/B \geq 1$ then loaded with $q = 40$ kPa. It is further noted in Figs. 6 and 7 that F reduces with increasing q. Considering the contour interval of the factor of safety with respect to the applied load, it can be observed that, the rate of decrease of F reduces for $q > 200$ kPa regardless of the footing location.

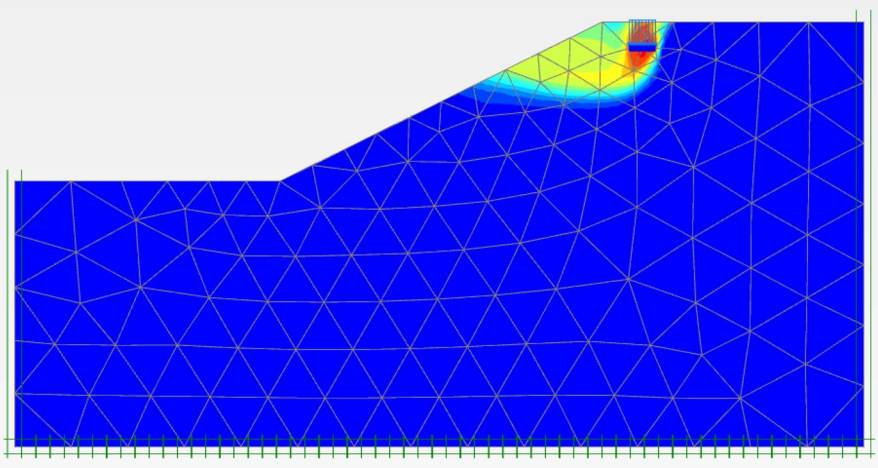

Fig. 5 Atypical finite element model with mesh and boundary conditions

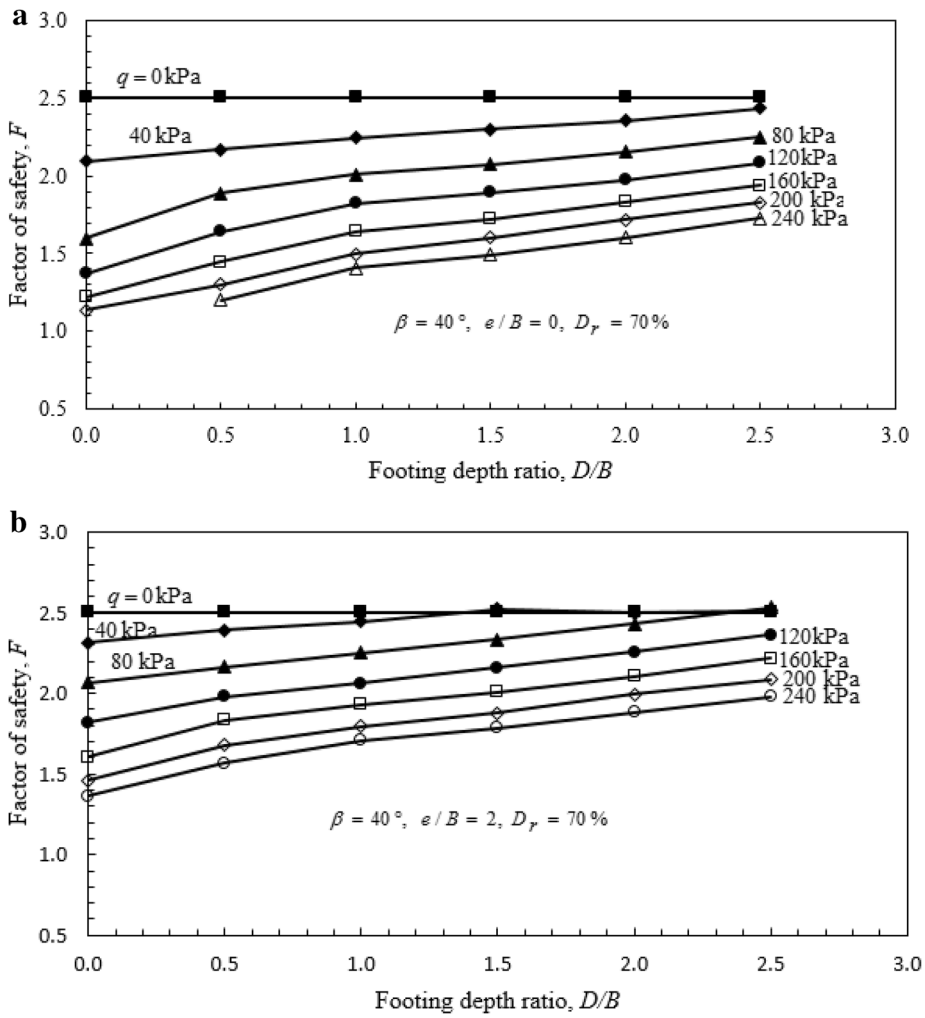

Fig. 6 Variation of factor of safety, F, with footing depth ratio D/B for 40° slope: **a** $e/B = 0$, **b** $e/B = 2$

Effect of footing edge distance

An analysis was carried out to determine the influence of the footing edge distance on the 40°, 50° and 60° slopes. In this case, $H = 6$ m, $B = 1$ m, and $D_r = 70\%$ were kept constant while the footing was loaded up to 240 kPa at edge distance ratio $e/B = 0$, 1, 2, 3, 4 for each D/B value of 0.0. 0.5, 1.0, 1.5 and 2.0. The variation of F with e/B for the various D/B values is presented in Fig. 8. It is observed that for $D/B = 0$ (footing on top of the crest), F improves with increasing e/B up to $e/B = 3$, then remains stable for $e/B > 3$. Thus, it can be stated that the maximum e/B, for the surface footing, beyond which the slope has a negligible effect on F is 3. Other researchers [9, 29, 35–40] who investigated the load bearing pressure of a footing on unreinforced and geosynthetic-reinforced slopes reported a trend comparable to the observation made in the present study. They found that the ultimate bearing capacity of the footing improved with increasing the footing edge distance from the crest. The maximum e/B within which the slope has a significant influence on the ultimate bearing capacity of the footing ranged from 2 to 5. It is again noted in Fig. 8 that when the footing is placed at $D/B \geq 0.5$, F improves steadily

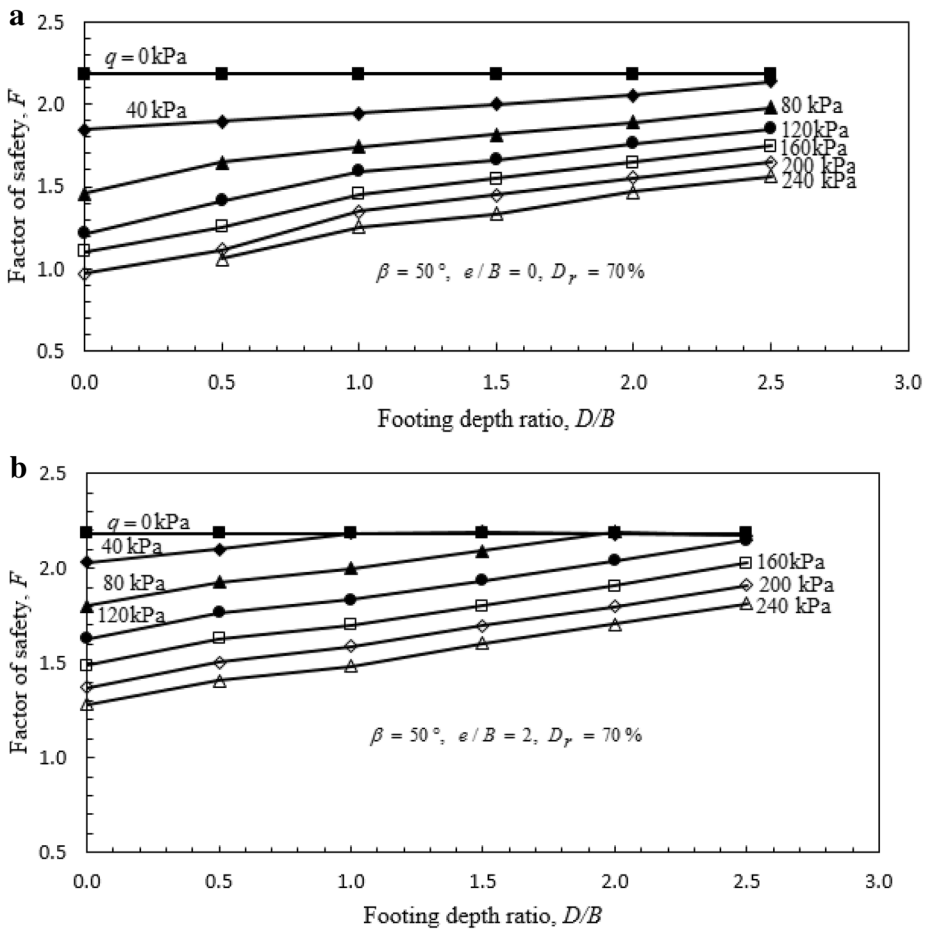

Fig. 7 Variation of factor of safety, *F*, with footing depth ratio *D*/*B* for 50° slope: **a** $e/B = 0$, **b** $e/B = 2$

with an increase in e/B. This observation is similar to the trend reported by Shields et al. [7] and Bauer et al. [14].

Effect of slope angle

In order to investigate the influence of the slope angle β on F, the footing, having a width $B = 1$ m, was positioned at each combination of $e/B = 0$, 1, 2, 3, 4 and $D/B = 0.0$, 0.5, 1.0, 1.5, 2.0, 2.5 in the 40°, 50° and 60° slopes having $H = 6$ m and $D_r = 70\%$. The values of q, applied to the footing, were varied from 0 to 240 kPa to observe the corresponding F for each slope angle. The variation of F with β for each D/B value is presented in Fig. 9. It is observed that F reduces with increasing β regardless of the footing depth and edge distance. This outcome agrees with the findings of Khan et al. [41] and Rai et al. [42] who respectively analysed the stability of a plastic pin-reinforced slope and a geogrid-reinforced mine waste dump and determined that the factor of safety reduced with increasing the slope inclination. The results, obtained in this study, are also consistent with the observation made by Lee and Manjunath [39], Choudhary et al. [37] and Keskin and Laman [9] while

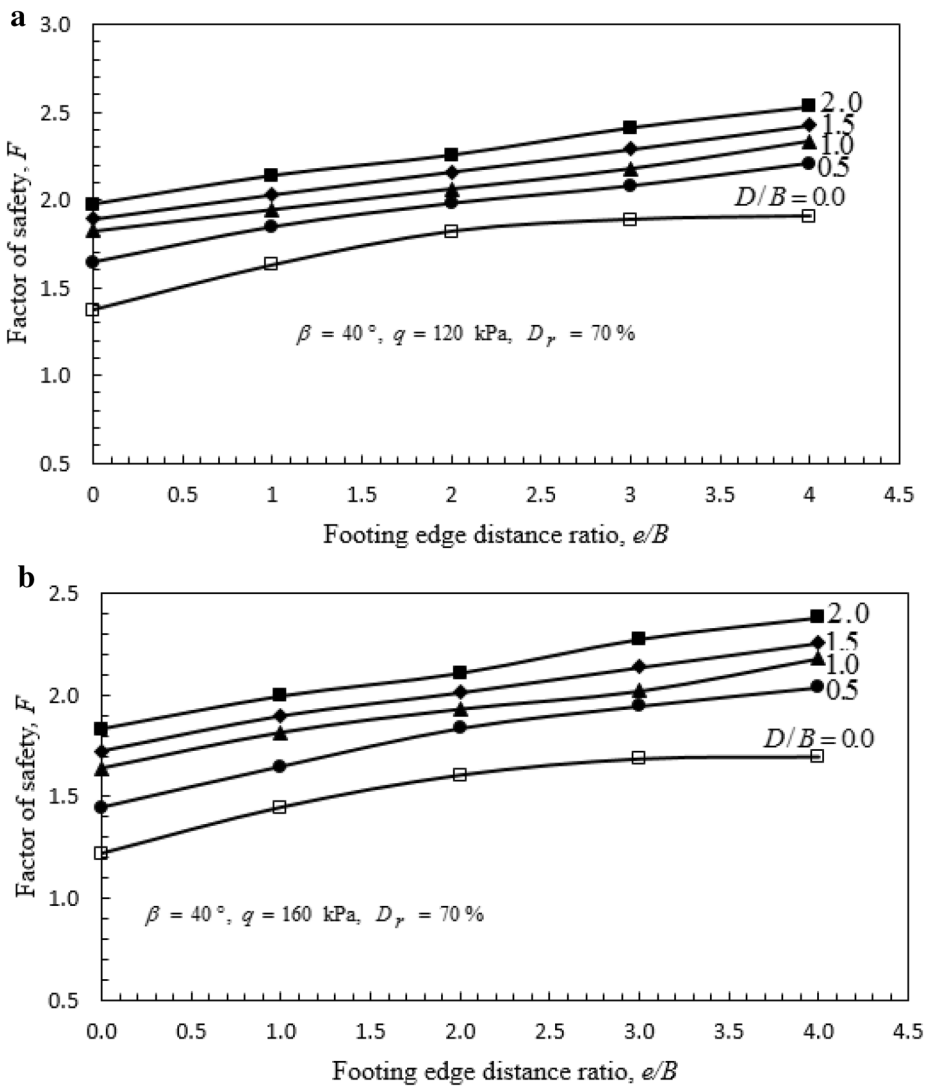

Fig. 8 Variation of factor of safety, F, with edge distance ratio, e/B: **a** $q = 120$ kPa, **b** $q = 160$ kPa

investigating the load-bearing capacity of a footing positioned on an unreinforced and a geosynthetic-reinforced slope crest. They found that the bearing capacity of the footing decreased with increasing the slope angle.

To overcome the reduction effect of the slope angle on F, the footing could be moved further away from the crest edge and/or below the crest into the slope. For example, in Fig. 9a, the factor of safety of the slope for a footing located at $D/B = 0$ and $e/B = 0$ reduces from 1.22 to 0.97 (becoming unstable) when the slope angle is increased from 40° to 60°. However, relocating the footing to $D/B = 0.5$ and $e/B = 2$ (Fig. 9b) in the 60° slope improves the factor of safety, by 54%, from 0.97 to 1.49. It is also demonstrated in Fig. 9b that having the footing at $D/B = 0$ and $e/B = 2$ in the 50° slope, as well as $D/B = 0.5$ and $e/B = 2$ in the 60° slope yields the same factor of safety.

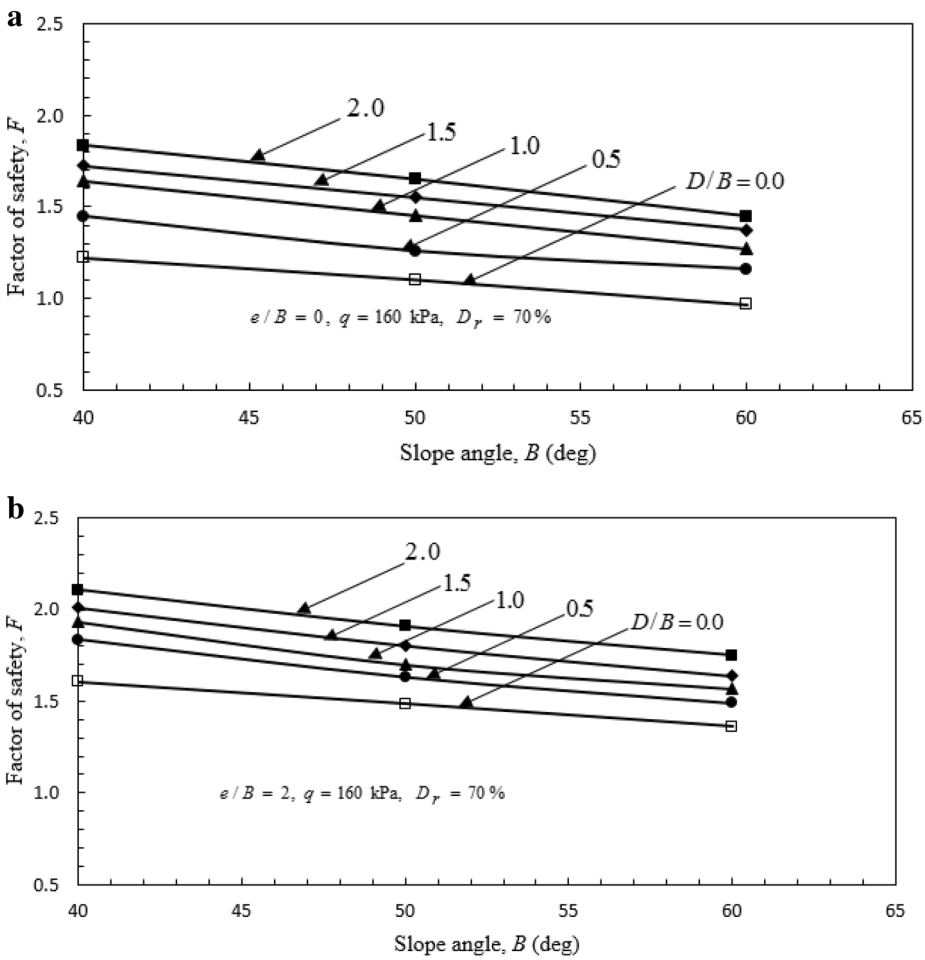

Fig. 9 Variation of factor of safety, F, with slope angle, β: **a** $e/B = 0$, **b** $e/B = 2$

Effect of relative density

Sandy soils have been classified into various density states ranging from loose to very dense based on the degree of compaction, which has a direct effect on the strength of the sand. To establish the relationship between the slope soil relative density (D_r = 50%, 70%, 90%) and F, the footing ($B = 1$ m) was placed within the slope, having a height $H = 6$ m and inclined at angles $\beta = 40°$, 50°, 60°, at the edge distance ratio, e/B of 0, 1, 2 and 3 for each depth ratio D/B of 0, 0.5, 1.0, 1.5 and 2. A pressure ranging from 120 to 200 kPa was applied to the footing at each footing location, defined by e/B and D/B, to observe the corresponding factor of safety. Figure 10 shows the relationship between F and D_r. It is noticed that F improves with increasing D_r from 50 to 70%, then the rate of improvement in F reduces for $D_r > 70\%$, regardless of the footing depth and edge distance. Keskin and Laman [9] observed, while studying the load-settlement performance of a footing placed on an unreinforced sand slope crest, that the ultimate bearing capacity of the footing improved with increasing the slope relative density. Kazi et al. [33] studied the effect of relative density on the bearing capacity of a footing on an unreinforced sand layer and determined a trend similar to that established in the present study.

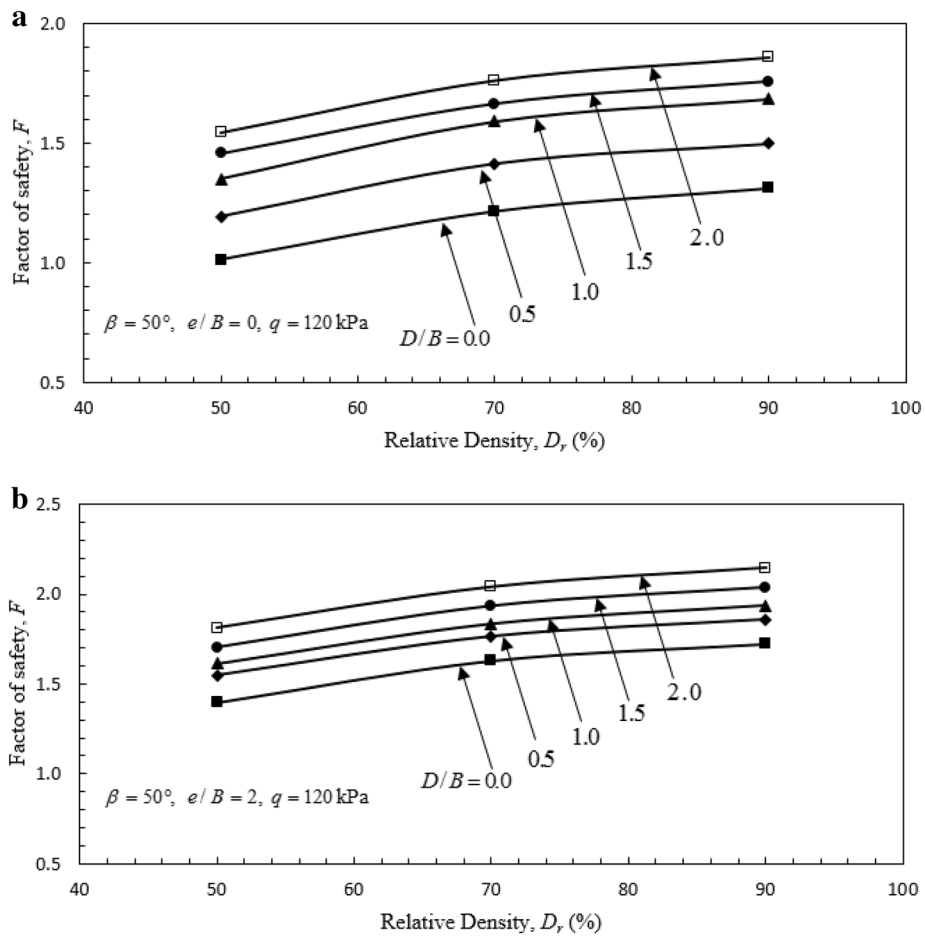

Fig. 10 Variation of factor of safety, F, with relative density, D_r: **a** $e/B = 0$, **b** $e/B = 2$

The improvement in F resulting from increasing the slope soil relative density D_r could be attributed to the fact that increasing D_r improves the shear strength of the slope which correspondingly increases the shearing resistance along the critical failure surface and hence improves the factor of safety. It is also noted that for a particular e/B and D_r, F increases with an increase in D/B. Combining e/B, D/B and D_r can significantly affect F. From Fig. 10a, $F=1$ when the footing is located at $e/B = 0$, $D/B = 0$ and the slope is compacted to a relative density $D_r = 50\%$. When the footing is placed below the crest at $e/B = 0$, $D/B = 0.5$, and D_r increases from 50 to 70% (Fig. 10a), F increases by 40% from 1 to 1.4. If the footing is again moved to $e/B = 2$, $D/B = 0.5$ and keeping $D_r = 70\%$ (Fig. 10b), F further increases by 40% to 1.8.

Failure zone and critical slip surface pattern

The stability (factor of safety) of a slope is very much related to the failure (shear) zone including the critical slip surface developed within the slope. The size of the failure zone and the corresponding length of the critical slip surface influence the shearing resistance along the failure surface. As the size of the shear zone and the length of the failure surface increase, the resistance to the footing failure offered by the shear zone, from the

slope face, and the shearing resistance along critical slip surface increase and enhance the overall stability of the slope. This section presents and discusses the typical pattern of shear zones and failure surfaces generated within the slope ($H = 6$ m and $D_r = 70\%$) as a result of varying the footing location (edge distance and depth) and the applied pressure. The footing width $B = 1$ m was used for the analysis.

Edge distance pattern

The critical failure surface developed from moving the footing away from the crest edge on the slope ($D/B = 0$) and within the slope ($D/B = 1$) are respectively displayed in Fig. 11a, b. The failure surfaces for the surface footing (Fig. 11a) start from the crest and end on the slope face for $e/B = 0$, 1, 2. The distance from the crest edge to the starting point of these slip surfaces on the crest increases with $e/B = 0$, 1, 2. However, these slip surfaces exit at the slope face with a decreasing distance from the crest. Figure 11a depicts that the overall size of the sliding wedges including the length of the failure surfaces for $e/B = 0$, 1, 2 increases from $e/B = 0$ to $e/B = 2$, with a corresponding improvement in F.

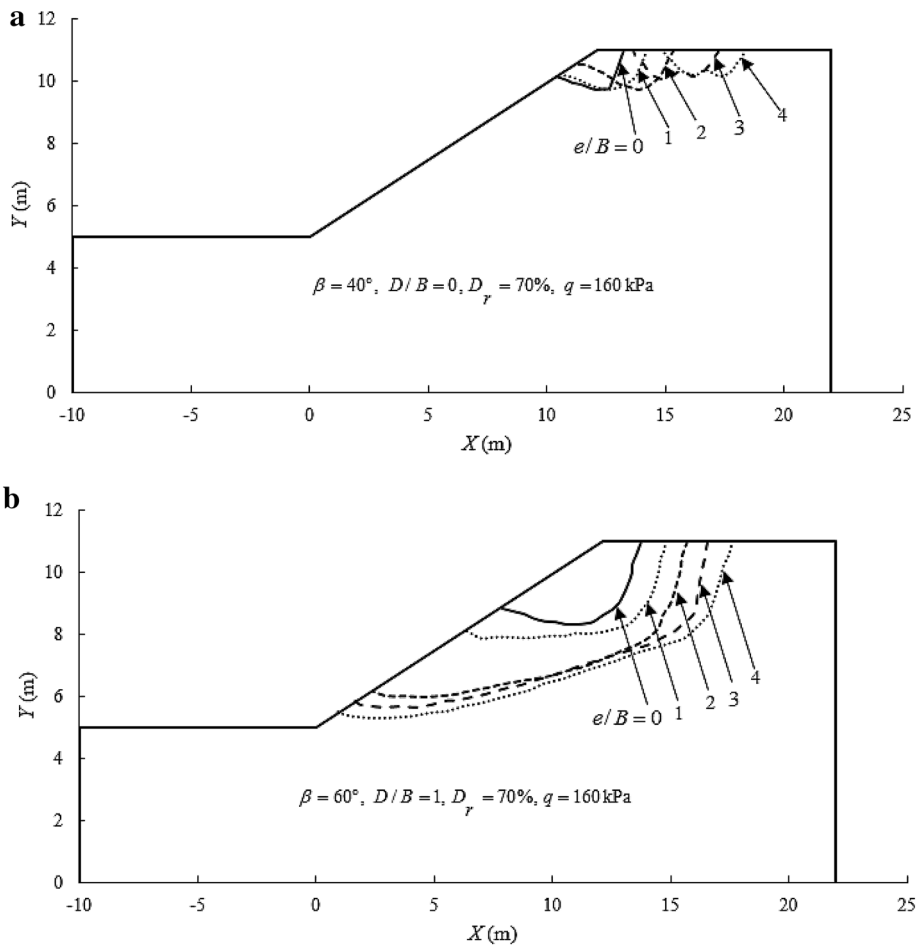

Fig. 11 Slip surface pattern with edge distance ratio, e/B: **a** $D/B = 0$, **b** $D/B = 1$

It is further observed that the slip surfaces generated for $e/B = 3, 4$ are different from those obtained for $e/B = 0, 1, 2$. The sliding surfaces for $e/B = 3, 4$ are symmetrical about the vertical axis, starting from a point within the slope and propagate to the crest. The size of the failure zone is almost the same for $e/B = 3, 4$ and larger than the size of the shear zones obtained for $e/B = 0, 1, 2$. Therefore the values of F obtained for $e/B = 3, 4$ are higher than those established for $e/B = 0, 1, 2$. It can be stated that the slip surfaces and shear zones for $e/B = 0, 1, 2$ are influenced by the slope and the crest whereas the sliding wedges for $e/B = 3, 4$ are entirely influenced by the crest (horizontal ground).

Figure 11b shows the pattern of failure surfaces and shear zones developed, from moving, the footing within the slope ($D/B = 1$), away from the crest edge at the edge distance ratio $e/B = 0, 1, 2, 3, 4$. It can be observed that the sliding surfaces, in this case, start from the crest and terminate on the slope face for all e/B values considered. The distance from the crest edge to the starting point of the slip surface on the slope crest and the distance from the crest to the ending point of the sliding surface along the slope face increases with increasing e/B from 0 to 4. Therefore, increasing e/B for a footing located below the crest increases the length of the sliding surface and size of the failure wedge and hence F. A comparison between the size of the failure zone for each e/B value presented in Fig. 11a, b, indicates that the size of the failure wedge for the embedded footing is larger than the surface footing for all e/B values considered for the analysis.

Embedment depth pattern

Figure 12 displays the pattern of sliding surfaces and failure zones generated from increasing the footing depth ($D/B = 0, 0.5, 1.0, 1.5, 2.0$) at $e/B = 1$. This failure pattern is similar to that observed from varying the footing edge distance $e/B = 0, 1, 2, 3, 4$ within the slope ($D/B = 1$) as shown in Fig. 11b. It can be clearly seen that as the footing depth ratio increases, the length of the slip surface and size of the shear zone increases and correspondingly improves F.

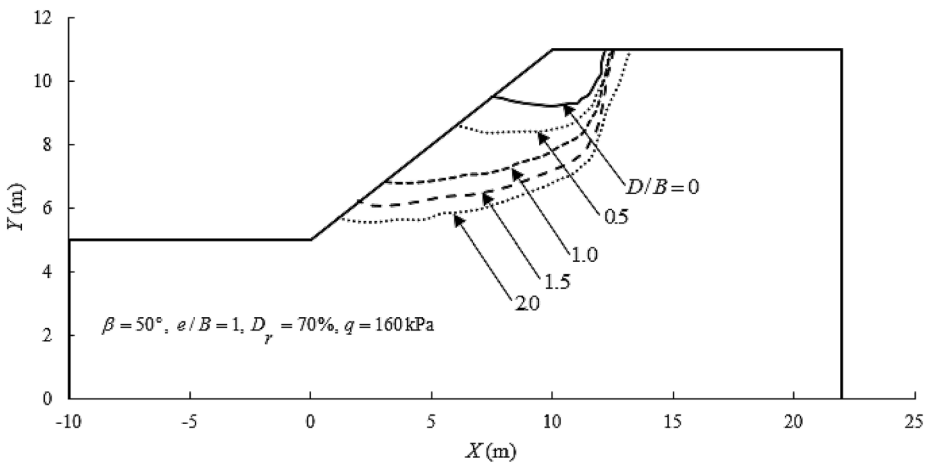

Fig. 12 Slip surface pattern with embedment depth ratio, D/B

Applied pressure pattern

Figure 13 presents the pattern of sliding surfaces and size of failure zones resulting from varying the footing applied pressure from $q = 0$ kPa to $q = 240$ kPa. It is observed that the slip surfaces for all the applied pressure considered, in the analysis, commence from almost the same location on the crest but end at different locations on the slope face, ascending the slope with increasing q. The length of the sliding surface and size of the sliding wedge reduce with an increase in q, resulting in a decrease in F.

Design charts

Slope design charts are tools used by geotechnical engineers for quick and preliminary assessment of slope stability. The estimated factor of safety from these charts can be used as a quality control check for detailed analysis. The charts can also be utilised in estimating the strength parameters of failed slopes for remedial works design [43].

Taylor [44] produced the first set of stability charts for unreinforced homogenous soil slopes without a loaded footing on the crest. Since then, several other charts for unreinforced slopes, not subjected to footing loads, have been developed by investigators [20, 44–52]. Review of previous works shows that design charts for estimating the factor of safety of slopes carrying embedded footing loads are limited. Consequently, it was considered to develop design charts for estimating the factor of safety of a 6-m high, 40°, 50° and 60°, slopes supporting a footing having a width $B = 1$ m, and subjected to a pressure $q = 100$ kPa. The locations of the footing considered are $e/B = 0$, 1, 2 and $D/B = 0$, 0.5, 1.0.

For each combination of e/B and D/B, the slope soil strength parameters c and ϕ were varied from 0 to 10 kPa and 30° to 50°, respectively to determine the resultant F for each slope angle. A dimensionless stability number (N) defined in Eq. (5) [48] was calculated for each analysis and the relation between F and N are presented as design charts in Figs. 14, 15, and 16.

$$N = c/\gamma H \tan\phi \tag{5}$$

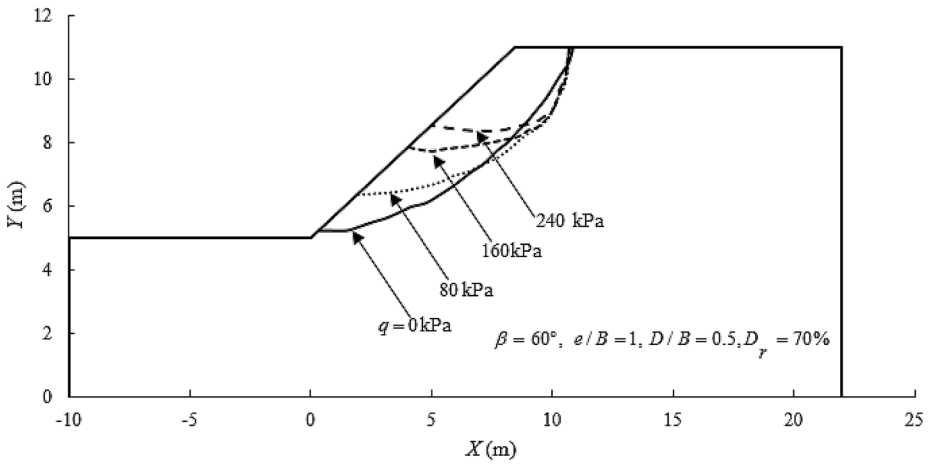

Fig. 13 Slip surface pattern with applied pressure, q

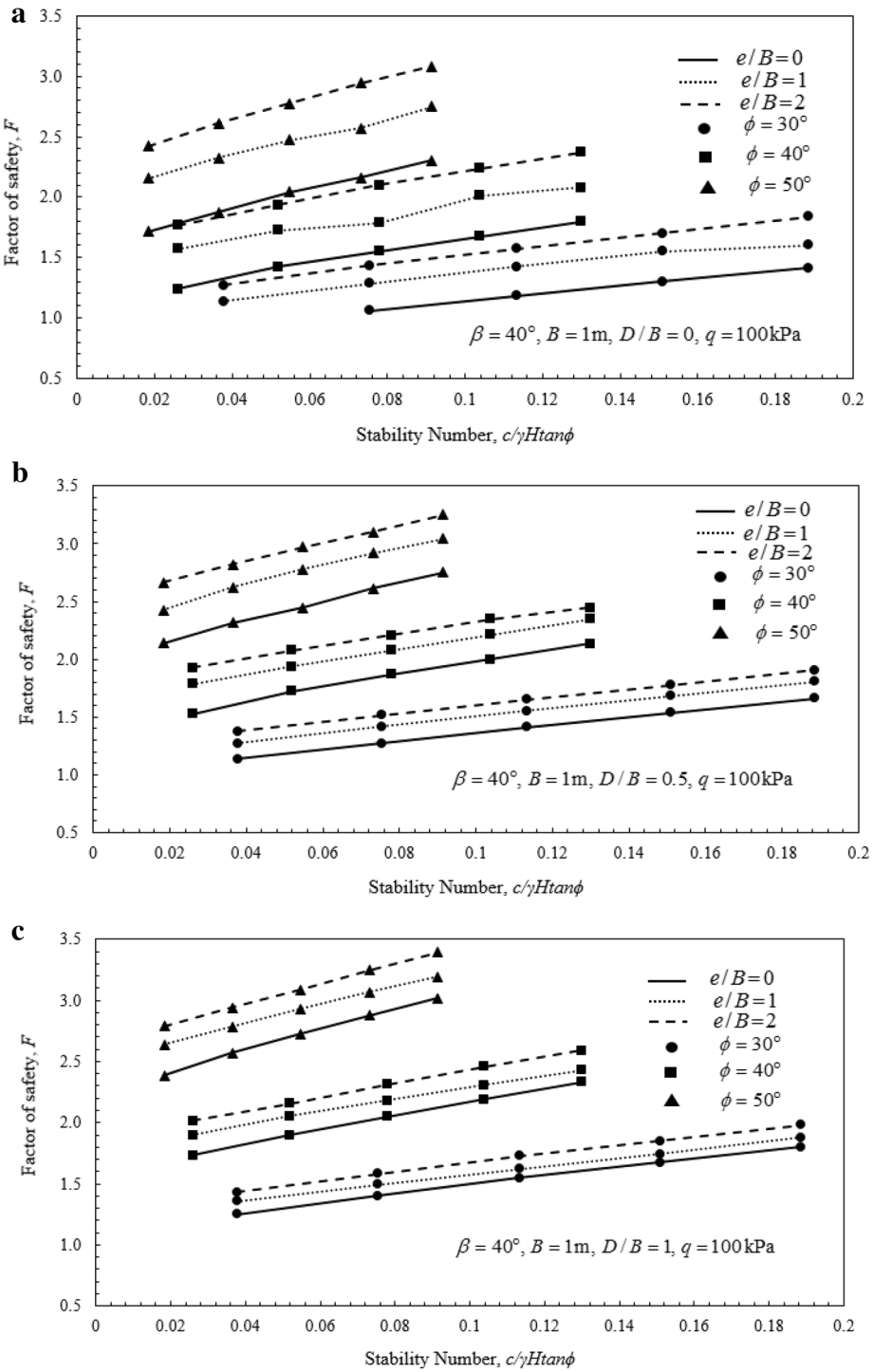

Fig. 14 Design charts for $\beta = 40°$: **a** $D/B = 0$, **b** $D/B = 0.5$, **c** $D/B = 1$

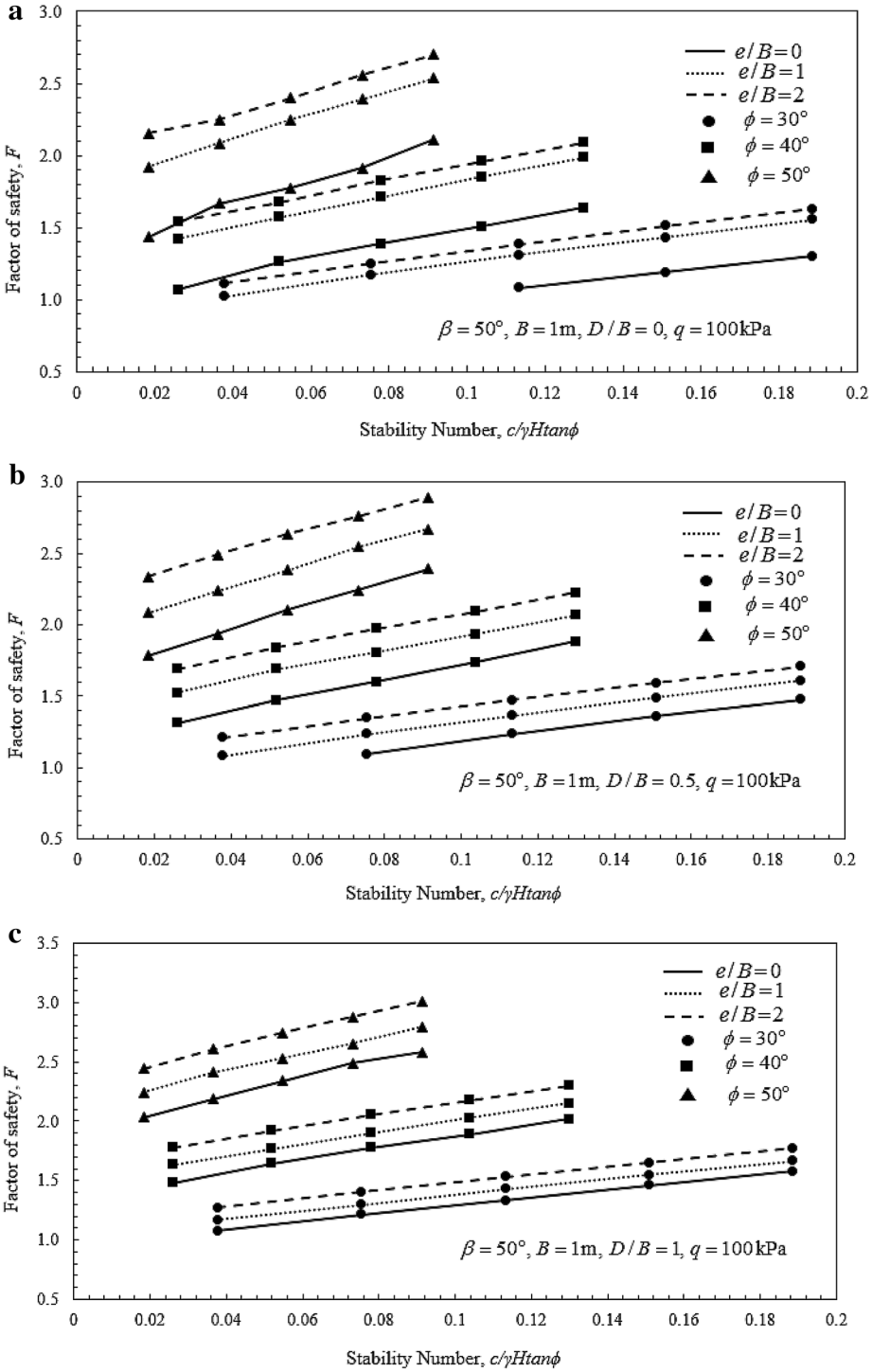

Fig. 15 Design Charts for $\beta = 50°$: **a** $D/B = 0$, **b** $D/B = 0.5$, **c** $D/B = 1$

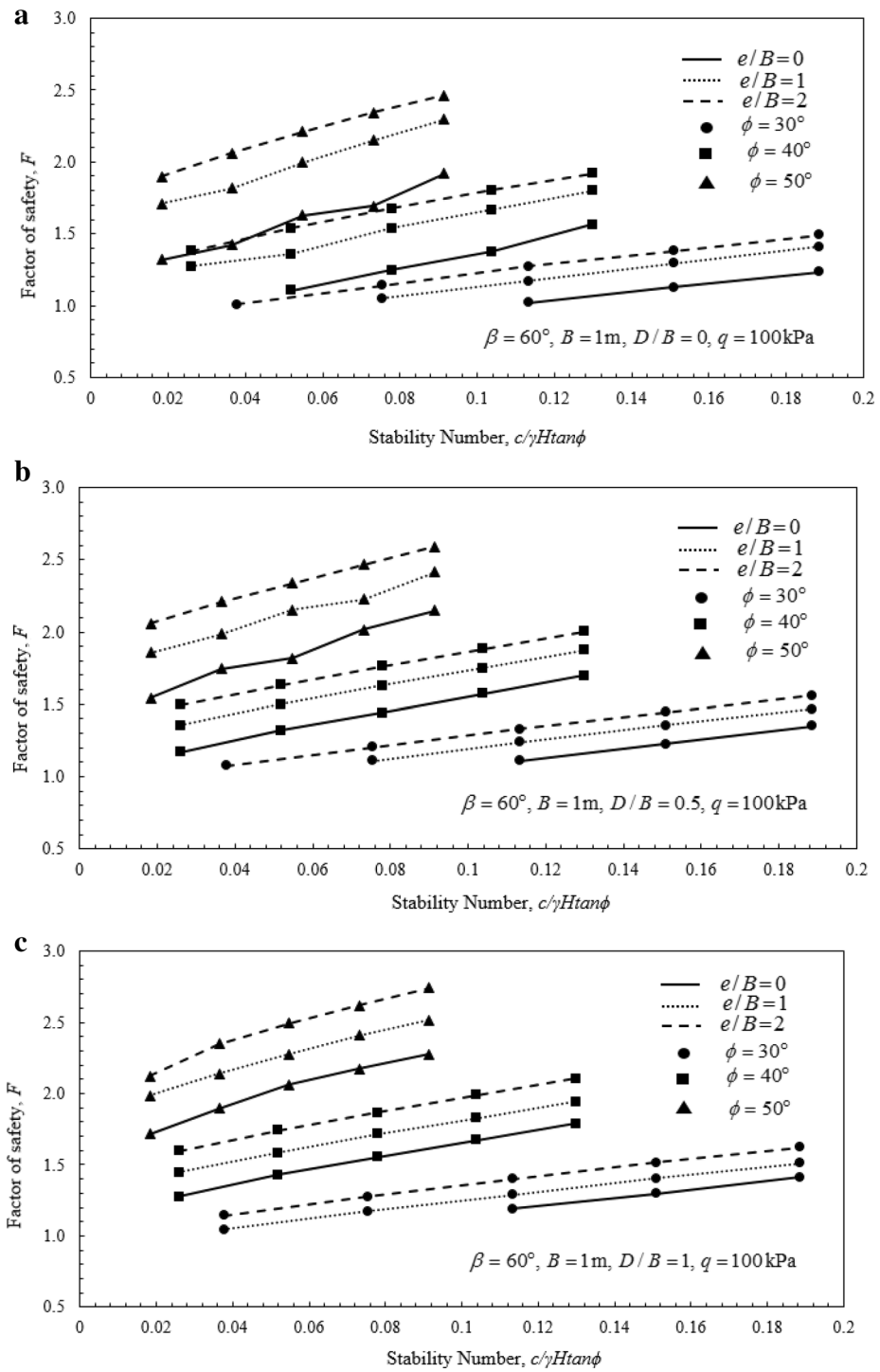

Fig. 16 Design Charts for $\beta = 60°$: **a** $D/B = 0$, **b** $D/B = 0.5$, **c** $D/B = 1$

It is observed that F improves with an increase in N values. When required, other design charts can be produced for various combination of soil strength, foundation depth, edge distance, slope angle and applied pressure following the methodology developed in this paper.

Illustrative example

An example is presented in this section to explain how the design charts presented in Figs. 14, 15, and 16 can be utilized by geotechnical engineers. Let us consider the following problem:

A footing having a width of 1 m is to be constructed on a slope crest, at a distance of 1 m from the crest edge. The footing pressure is $q = 100$ kPa. Consider the following: $H = 6$ m, $\beta = 50°$, $\gamma = 15.3$ kN/m^3, $c = 3$ kPa and $\phi = 35°$. Determine the factor of safety of the slope.

Solution

From Eq. (5),

$$N = \frac{c}{\gamma H \tan\phi} = \frac{3}{(15.3)(6)(\tan 35)} = 0.05.$$

Using the slope angle, $\beta = 50°$, the footing edge distance ratio $e/B = 1$, and the footing depth ratio $D/B = 0$, the factor of safety of the slope can be estimated from Fig. 15a as $F = 1.3$, which indicates that the slope is stable.

Conclusions

The stability analysis of a sandy slope supporting an embedded footing has been evaluated by developing a numerical model with focus on the factor of safety. A series of 2D finite element analysis has been conducted to determine the effect of the following parameters on the factor of safety (F) of the slope: slope angle (β), relative density (D_r), footing edge distance (e), footing depth (D) and applied pressure (q). Based on the results and discussion, the following conclusions can be drawn:

- The factor of safety (F) of the slope reduces with an increase in the applied footing pressure and the slope angle.
- Increasing the footing depth ratio (D/B) improves F irrespective of the slope angle (β) and the edge distance ratio (e/B).
- The slope stability also improves with increasing footing edge distance ratio (e/B), regardless of the slope angle (β) and the depth ratio (D/B). For a surface footing, F increases to a critical value at $e/B = 3$ then remains constant for $e/B > 3$.
- As the relative density (D_r) increases, F significantly improves until $D_r = 70\%$ beyond which further increase in D_r results in a marginal increase in F.
- Design charts for estimating F for 40°, 50° and 60° slopes, having a height $H = 6$ m, and supporting an embedded footing with parameters $q = 100$ kPa, $e/B = 0$, 1, 2, $D/B = 0$, 0.5, 1.0, and $B = 1$ m have been provided. An illustrative example has been given to explain how the developed charts can be utilized by the geotechnical/civil engineers. As required, the design charts for other cases may be created following the methodology developed in this paper.

Authors' contributions
EBF carried out numerical modelling of the research problem, and presented the results in graphical forms. SKS worked with EBF to analyze the results and presented the discussion along with an illustrative example. Both authors read and approved the final manuscript.

Competing interests
The authors declare that there is no competing interests.

Publisher's Note

Received: 23 April 2018 Accepted: 20 August 2018
Published online: 11 September 2018

References
1. Buhan PD, Garnier D (1998) Three dimensional bearing capacity analysis of a foundation near a slope. Soils Found 38(3):153–163
2. Castelli F, Motta E (2010) Bearing capacity of strip footings near slopes. Geotech Geol Eng 28(2):187–198
3. Graham J, Andrews M, Shields DH (1988) Stress characteristics for shallow footings in cohesionless slopes. Can Geotech J 25(2):238–249
4. Meyerhof GG (1957) The ultimate bearing capacity of foundations on slopes. Proc IV Int Conf Soil Mech Found Eng England 1:384–387
5. Narita K, Yamaguchi H (1990) Bearing capacity analysis of foundations on slopes by use of log-spiral sliding surfaces. Soils Found 30(3):144–152
6. Saran S, Sud VK, Handa SC (1989) Bearing capacity of footings adjacent to slopes. J Geotech Eng 115(4):553–573
7. Shields DH, Scott JD, Bauer GE, Deschemes JH, Barsvary A. K (1977) Bearing capacity of foundations near slopes. In: Proceedings of the 9th international conference on soil mechanics and foundation engineering, Tokyo, pp 715–20
8. Castelli F, Lentini V (2012) Evaluation of the bearing capacity of footings on slopes. Int J Phys Model Geotech 12(3):112–118
9. Keskin MS, Laman M (2013) Model studies of bearing capacity of strip footing on sand slope. KSCE J Civil Eng 17(4):699–711
10. Patil VN, Chore HS (2017) Bearing capacity behaviour of a strip footing on model slopes made up of fly ash and furnace slag. Int J Geotech Eng 11(15):431–440
11. Acharyya R, Dey A (2017) Finite element investigation of the bearing capacity of square footings resting on sloping ground. INAE Lett 2(3):97–105
12. Georgiadis K (2010) Undrained bearing capacity of strip footings on slopes. J Geotech Eng 136(5):677–685
13. Zhou H, Zheng G, Yin X, Jia R, Yang X (2018) The bearing capacity and failure mechanism of a vertically loaded strip footing placed on the top of slopes. Comput Geotech 94:12–21
14. Bauer GE, Shields DH, Scot JD, Gruspier JE (1981) Bearing capacity of footing in granular slope. In: Proceedings of the 11th international conference on soil mechanics and foundation engineering, The Netherlands, pp 33–36
15. Chang Y, Huang T (2005) Slope stability analysis using strength reduction technique. J Chin Instit Eng 28(2):231–240
16. Hammouri NA, Husein MAI, Yamin MMA (2008) Stability analysis of slopes using the finite element method and limiting equilibrium approach. Bull Eng Geol Environ 67(4):471–478
17. Matteo LD, Valigi D, Ricco R (2013) Laboratory shear strength parameters of cohesive soils: variability and potential effects on slope stability. Bull Eng Geol Env 72(1):101–106
18. Kelesoglu MK (2016) The evaluation of three-dimensional effects on slope stability by the strength reduction method. KSCE J Civil Eng 20(1):229–242
19. Brinkgreve RB, Kumarswamy S, Swolfs WM (2016) Plaxis 2D–3D overview of the full manual-general information. Delft University of Technology, Delft
20. Chok YH, Jaksa MB, Kaggwa WS, Griffiths DV (2015) Assessing the influence of root reinforcement on slope stability by finite elements. Int J Geo-Eng 6(1):1–13
21. Alamshahi S, Hataf N (2009) Bearing capacity of strip footings on sand slopes reinforced with geogrid and grid-anchor. Geotext Geomembr 27(3):217–226
22. Noorzad R, Manavirad E (2014) Bearing capacity of two close strip footings on soft clay reinforced with geotextile. Arab J Geosci 7(2):623–639
23. Griffiths DV, Lane PA (1999) Slope stability analysis by finite elements. Geotechnique 49(3):387–403
24. Hammah RE, Yacoub TE, Corkum B, Curran JH (2005) A comparison of finite element slope stability analysis with conventional limit-equilibrium investigation. In: Proc. 58th Canadian geotechnical and 6th joint IAH-CNC and CGS groundwater specialty conferences, GeoSask 2005, Saskatoon, pp 480–487
25. Cheng YM, Lansivaara T, Wei WB (2007) Two-dimensional slope stability analysis by limit equilibrium and strength reduction methods. Comput Geotech 34(3):137–150
26. Bhattacherjee Bhattacherjee D, Viswanadham BVS (2015) Numerical studies on the performance of hybrid-geosynthetic-reinforced soil slopes subjected to rainfall. Geosynth Int 22(6):411–427
27. Tiwari G, Samadhiya NK (2016) Factors Influencing the distribution of peak tension in geosynthetic reinforced soil slopes. Indian Geotech J 46(1):34–44
28. Vali R, Saberian M, Li J, Sham G, Van Gelder P (2017) Properties of geogrid-reinforced-marine-slope due to the groundwater level changes. Marine Georesour Geotechnol. 36:1–14

29. Gill KS, Shukla SK, Jha JN, Choudhary AK (2013) Experimental and numerical studies of loaded strip footing resting on reinforced fly ash slope. Geosynth Int 20(1):13–25
30. Zornberg JG, Sitar N, Mitchell J (1998) Limit Equilibrium as a basis for design of geosynthetic reinforced slopes. J Geotech Geoenviron Eng 124(8):684–698
31. Zornberg JG, Sitar N, Mitchell JK (1998) Performance of geosynthetic reinforced slopes at failure. J Geotech Geoenviron Eng 124(8):670–683
32. Kazi M, Shukla SK, Habibi D (2015) An improved method to increase the load-bearing capacity of strip footing resting on geotextile-reinforced sand bed. Indian Geotech J 45(1):98–109
33. Kazi M, Shukla SK, Habibi D (2016) Behaviour of an embedded footing on geotextile-reinforced sand. Ground Improv 169(2):120–133
34. Patra CR, Das BM, Atalar C (2005) Bearing capacity of embedded strip foundation on geogrid-reinforced sand. Geotext Geomembr 23(5):454–462
35. Shin EC, Das BM, Lee ES, Atalar C (2002) Bearing capacity of strip foundation on geogrid-reinforced sand. J Geotechn Geol Eng 20(2):169–180
36. Altalhe EB, Taha MR, Abdrabbo FM (2015) Behavior of strip footing on reinforced sand slope. J Civil Eng Manag 21(3):376–383
37. Choudhary AK, Jha JN, Gill KS (2010) Laboratory investigation of bearing capacity behaviour of strip footing on reinforced flyash slope. Geotext Geomembr 28(4):393–402
38. El Sawwaf MA (2007) Behavior of strip footing on geogrid-reinforced sand over a soft clay slope. Geotext Geomembr 25(1):50–60
39. Lee KM, Manjunath VR (2000) Experimental and numerical studies of geosynthetic-reinforced sand slopes loaded with a footing. Can Geotech J 37(4):828–842
40. Rao SVK, Nasr AMA (2010) Experimental and theoretical studies of vertical piles reinforced sand slopes loaded with strip footing. Geotech Test J 33(5):385–396
41. Khan M, Hossain MDS, Ahmed A (2017) Parametric study on slope stability using recycled plastic pin. In: 6th International symposium on geotechnical safety and risk. Canada, 226–236
42. Rai R, Khandelwal M, Jaiswal A (2012) Application of geogrids in waste dump stability: a numerical modeling approach. Environ Earth Sci 66(5):1459–1465
43. Abramson LW, Lee TS, Sharma S, Boyce GM (2002) Slope stabilisation and stabilisation methods, 2nd edn. Willey, New York
44. Taylor DW (1937) Stability of earth slopes. J Boston Soc Civil Eng 24:337–386
45. Baker R (2003) A second look at Taylor's stability chart. J Geotech Geoenviron Eng 129(12):1102–1108
46. Lim K, Lyamin AV, Cassidy MJ, Li AJ (2015) Three-dimensional slope stability charts for frictional fill Materials placed on purely cohesive clay. Int J Geomech 16(2):1–8
47. Michalowski RL (2010) Limit analysis and stability charts for 3D slope failures. J Geotech Geoenviron Eng 136(4):583–593
48. Michalowski RL (2002) Stability charts for uniform slopes. J Geotech Geoenviron Eng 128(4):351–355
49. Moregenstern N (1963) Stability charts for earth slopes during rapid drawdown. Géotechnique 13(2):121–131
50. Qian ZG, Li AJ, Merifield RS, Lyamin AV (2014) Slope stability charts for two-layered purely cohesive soils based on finite-element limit analysis methods. Int J Geomech 15(3):1–14
51. Sun J, Zhao Z (2013) Stability charts for homogenous soil slopes. J Geotech Geoenviron Eng 139(12):2212–2218
52. Wang L, Shi P, Tian H, Cao L, Huang Y, Xue F (2016) Stability analysis and charts for borrowed soil in ecological slope engineering. Indian Geotech J 46(4):425–436